Proc. of SPIE Vol. 0518, Optical Systems Engineering IV, ed. P.R. Yoder, Jr. (Oct 1984) Copyright SPIE

Non-symmetric thermal bowing of flat circular mirrors

Pravin K. Mehta

Electro-Optical Division, Perkin-Elmer Corporation,
Mail Station 955
100 Wooster Heights Road, Danbury, Connecticut, 06810

Abstract

This paper presents a closed form solution of the biharmonic differential equation for the bending of a thin circular plate, which is kinematically supported and subjected to a generalized non-uniform thermal moment distribution. From this solution, normalized performance curves are developed for nonuniform thermal bowing and the ensuing RMS figure errors in flat circular mirrors. Several test cases of the closed form solutions were compared with independent Nastran based finite element solutions, and practically exact correlation between the two was obtained in all the cases. However, an analytical approach based on the closed form solution is significantly more efficient and cost-effective. The methodology of the closed form solution is not limited to flat circular mirrors. Some illustrative examples are included here from a similar, but somewhat more complex, closed form solution for curved circular mirrors.

Introduction

Several thermoelastic distortion effects combine to produce the mirror surface or figure distortion in response to applied thermal loads. Usually, the major effect is that of thermal "bowing", which is due to the bending about the mirror neutral surface. In the case of a lightweighted construction, the facesheet also bends about its own neutral surface causing "quilting". The mirror, being a 3-dimensional elastic continum, also experiences an intrinsic lateral restraint due to the existence of Poisson's ratio. This lateral restraint together with the "thermal growth" constitute the "axial strain" effect. It is a common practice in opto-structural engineering to calculate these thermal distortion effects separately and obtain the resultant surface distortion by superposition. In this paper, we will confine our attention to thermal bowing, which is usually the major contributor to overall thermal distortion of a mirror.

The thermal bowing of a flat circular mirror is governed by the biharmonic differential equation[1]

$$\nabla^2\nabla^2 w = \frac{a^2}{D(\nu-1)}\nabla^2 M_T \qquad (1)$$

where

∇^2 = Laplacian operator

$$= \frac{\partial^2}{\partial\rho^2} + \frac{1}{\rho}\frac{\partial}{\partial\rho} + \frac{1}{\rho^2}\frac{\partial^2}{\partial\theta^2} \qquad (2)$$

ρ = normalized radial coordinate = r/a

r = radial coordinate

a = outer radius of the plate

w = plate deflection

M_T = thermal moment

D = flexural rigidity of the plate

ν = Poisson's ratio

Since the mirror is assumed to be kinematically supported, the support reaction forces are zero. The analysis is then applicable to lightweighted mirrors by using appropriate cross sectional moment of inertia in the calculation of flexural rigidity D, because the transverse shear deflection is only due to nonuniform thermal moment, and that happens to be either zero or relatively small.

Before proceeding with the thermal bowing analysis, it is convenient to define the analytical nomenclature as follows:

b = plate central hole radius

c = inner radius of the heated aperture

d = outer radius of the heated aperture

s = pitch circle radius of the 3-point kinematic mount

m = radial index of thermal moment distribution

n = azimuthal index of thermal moment distribution

h = subscript denoting homogeneous solution (of the differential equation)

p = subscript denoting particular integral

z = axial coordinate measured from neutral surface

E = Young's modulus

I = moment of inertia of plate cross section per unit width

T = temperature

M_r = radial bending moment

M_t = tangential bending moment

M_{rt} = torsional moment

Q_r = radial transverse shear force

Q_t = tangential transverse shear force

V = support reaction

} These are stress resultants per unit length

α = coefficient of thermal expansion

θ = azimuthal coordinate

μ = thermal moment coefficient for Cosine series

ξ = thermal moment coefficient for Sine series

ρ_b = b/a

ρ_c = c/a

ρ_d = d/a

ρ_s = s/a

The inner radius c and the outer radius d of the heated aperture allude to the possibility of the heated aperture being somewhat smaller than the full aperture as illustrated in Figure 1.

Thermal moment distribution

The thermal moment M_T is given by

$$M_T = \int_z \left[\int_{T_o}^{T_z} E\,\alpha dT\right] z dz, \tag{3}$$

where

T_o = reference temperature at which the plate is free from thermal stresses and deformation

T_z = temperature at a distance z from the neutral surface of the plate

= $T_z(\rho,\theta)$, a function of ρ and θ.

In the temperature range of practical interest, the variation of Young's modulus E with temperature is quite small for most materials and may be justifiably ignored. The coefficient of expansion α, on the other hand, varies significantly. Figure 2 illustrates this for ULE. Let $\alpha = f(T)$ be integrable in the temperature range of interest, so that

$$\int E\alpha dT = E\int \alpha dT, = E\int f(T)dT = E\phi(T) \tag{4}$$

say. Then

$$\int_{T_o}^{T_z} \alpha dT = \phi(T_z) - \phi(T_o) = \phi\left(T_z(\rho,\theta)\right) - \phi(T_o) \tag{5}$$

The integral in Eq. (5) represents the free thermal strain ϵ_T, or $\Delta L/L$ as commonly known. For ULE, the variation of $\Delta L/L$ with temperature, assuming $T_o = 20^oC$, is illustrated in Figure 3.

Since E is assumed to be constant, we have by substituting for the integral from (5) into (3),

$$M_T = M_T(\rho,\theta) = E\int_z \phi(T_z) z dz - E\phi(T_o)\int_z z dz \tag{6}$$

It may be noted that $\int_z z dz = 0$ for those cross sections, which are symmetric with respect to the neutral surface. If the temperature distribution $T_z(\rho,\theta)$ is known, say, from a heat transfer analysis, then the thermal moment distribution $M_T(\rho,\theta)$ can be calculated by means of Eq. (6).

For the purpose of solving the biharmonic differential Eq. (1), it is desirable to express M_T in a deterministic form. This may be done by a numerical analysis of the thermal moment data at a number of points in the mirror. A very useful representation of the thermal moment distribution may be taken in the form of the following double series.

$$M_T = \sum_{m=o}^{M}\sum_{n=o}^{\infty} (\mu_{mn}\cos n\theta + \xi_{mn}\sin n\theta)\,\rho^m, \tag{7}$$

where coefficients μ_{mn} and ξ_{mn} are determined from a numerical analysis. An advantage of using ρ^m in this representation of M_T is that a number of other types of functions can be constructed by appropriate combinations of various powers of ρ. For example, the circular and hyperbolic sine and cosine of $k\pi\rho$ (where k is any integer), the Zernike polynomials, etc. may be constructed from (7). Accordingly, for the nonsymmetric thermal bowing problem under consideration, the thermal moment distribution will be assumed to be given by Eq. (7).

The general solution

By operating ∇^2, defined in Eq. (2) on M_T given by Eq. (7), we have

$$\nabla^2 M_T = \sum_{m=0}^{M}\sum_{n=0}^{\infty}\cdot \left[(\mu_{mn}\cos n\theta + \xi_{mn}\sin n\theta) \times (m^2 - n^2)\rho^{m-2}\right] \tag{8}$$

Therefore, the biharmonic differential Eq. (1) becomes

$$\nabla^2\nabla^2 w = \frac{a^2}{D(\nu-1)}\sum_{m=0}^{M}\sum_{n=0}^{\infty}\left[(\mu_{mn}\cos n\theta + \xi_{mn}\sin n\theta)\,(m^2 - n^2)\,\rho^{m-2}\right] \tag{9}$$

The general solution of this equation is given by

$$w = \frac{1}{D(\nu-1)}\sum_{n=0}^{\infty}\left[(w_{h_n} + w_{p_n})\cos n\theta + (\hat{w}_{h_n} + \hat{w}_{p_n})\sin n\theta\right] \tag{10}$$

where the cos $n\theta$ and sin $n\theta$ terms respectively imply symmetric and anti-symmetric stress-deflection systems with respect to the azimuthal reference $\theta = 0$, and

$$w_{h_o} = A_o + B_o\rho^2 + C_o \ell n\,\rho + D_o\rho^2 \ell n\,\rho \tag{11}$$

$$w_{h_1} = A_1\rho + B_1\rho^3 + C_1\rho^{-1} + D_1\rho \ell n\,\rho \tag{12}$$

$$w_{h_n} = A_n\rho^n + B_n\rho^{n+2} + C_n\rho^{-n} + D_n\rho^{-(n-2)}, \quad \text{when } n \geq 2 \tag{13}$$

$$\hat{w}_{h_1} = \hat{A}_1\rho + \hat{B}_1\rho^3 + \hat{C}_1\rho^{-1} + \hat{D}_1\rho \ln \rho \tag{14}$$

$$\hat{w}_{h_n} = \hat{A}_n\rho^n + \hat{B}_n\rho^{n+2} + \hat{C}_n\rho^{-n} + \hat{D}_n\rho^{-(n-2)}, \quad \text{when } n \geq 2 \tag{15}$$

$$w_{p_n} = a^2 \sum_{m=0}^{M} \mu_{mn} \frac{\rho^{m+2}}{(m+2)^2 - n^2}, \quad \text{when } n \neq m+2 \tag{16}$$

$$w_{p_n} = a^2 \sum_{m=0}^{M} \mu_{mn} \frac{(\ln \rho)\,\rho^{m+2}}{2(m+2)}, \quad \text{when } n = m+2 \tag{17}$$

$$\hat{w}_{p_n} = a^2 \sum_{m=0}^{M} \xi_{mn} \frac{\rho^{m+2}}{(m+2)^2 - n^2}, \quad \text{when } n \neq m+2 \tag{18}$$

$$\hat{w}_{p_n} = a^2 \sum_{m=0}^{M} \xi_{mn} \frac{(\ln \rho)\,\rho^{m+2}}{2(m+2)}, \quad \text{when } n = m+2 \tag{19}$$

and $A_o, B_o, \ldots, \hat{C}_n, \hat{D}_n$ are integration constants.

Since the resulting analytical formulas for the cos $n\theta$ and sin $n\theta$ terms are very similar, all of the subsequent analytical derivation will be given for the cos $n\theta$ terms only.

The integration constants and heat load for the three regions shown in Figure 1 are different. Table 1 defines the notation used for the three corresponding sets of integration constants, deflection and stress resultants, and also identifies the heat loads in terms of the thermal moment coefficients.

Table 1. Matrix of integration constants, deflection functions, stress resultants, and thermal moment coefficients for the three regions defined in Figure 1.

	Region	Integration Constants	Deflection and Stress Resultants	Thermal Moment Coefficients
1	$\rho_b \leq \rho \leq \rho_c$	$\underline{A}_o, \underline{B}_o, \underline{C}_o, \underline{D}_o$ $\underline{A}_1, \underline{B}_1, \underline{C}_1, \underline{D}_1$ $\underline{A}_n, \underline{B}_n, \underline{C}_n, \underline{D}_n$	$\underline{w}$, $\underline{M}_r$, $\underline{M}_t$ $\underline{M}_{rt}$, $\underline{Q}_r$, $\underline{Q}_t$, $\underline{V}$, etc.	$\mu_{mn} = 0$
2	$\rho_c \leq \rho \leq \rho_d$	A_o, B_o, C_o, D_o A_1, B_1, C_1, D_1 A_n, B_n, C_n, D_n	w, M_r, M_t M_{rt}, Q_r, Q_t, V, etc.	$\mu_{mn} \neq 0$
3	$\rho_d \leq \rho \leq 1$	$\overline{A}_o, \overline{B}_o, \overline{C}_o, \overline{D}_o$ $\overline{A}_1, \overline{B}_1, \overline{C}_1, \overline{D}_1$ $\overline{A}_n, \overline{B}_n, \overline{C}_n, \overline{D}_n$	$\overline{w}$, $\overline{M}_r$, $\overline{M}_t$ $\overline{M}_{rt}$, $\overline{Q}_r$, $\overline{Q}_t$, $\overline{V}$, etc.	$\mu_{mn} = 0$

Stress resultants (cos nθ terms)

The stress resultants are obtained by substituting various partial derivatives of w with respect to r and θ into the respective formulas[1] for stress resultants. The results of the derivation are given below. There are four cases to be considered for each of the three regions defined in Figure 1: (i) n = 0; (ii) n = 1; (iii) $n \geq 2$, when $n \neq m + 2$; (iv) $n \geq 2$, when $n = m + 2$.

Middle region ($\rho_c < \rho < \rho_d$): First for n = 0, we have

$$\frac{\partial w_c}{\partial r} = \frac{1}{D(\nu-1)a}\left[2B_o\rho + \frac{C_o}{\rho} + D_o\rho(1 + 2\,\ell n\,\rho) + a^2\sum_{m=0}^{M}\mu_{mo}\frac{\rho^{m+1}}{m+2}\right] \tag{20}$$

$$\frac{\partial^2 w_c}{\partial r^2} = \frac{1}{D(\nu-1)a^2}\left[2B_o - \frac{C_o}{\rho^2} + D_o(3 + 2\,\ell n\,\rho) + a^2\sum_{m=0}^{M}\mu_{mo}\frac{m+1}{m+2}\rho^m\right] \tag{21}$$

$$M_{r_o} = \frac{1}{(1-\nu)a^2}\left[2B_o(1+\nu) - C_o\frac{1-\nu}{\rho^2} + D_o\{(3+\nu) + 2(1+\nu)\,\ell n\,\rho\} - (1-\nu)a^2\sum_{m=0}^{M}\mu_{mo}\frac{\rho^m}{m+2}\right] \tag{22}$$

$$M_{t_o} = \frac{1}{(1-\nu)a^2}\left[2B_o(1+\nu) + C_o\frac{1-\nu}{\rho^2} + D_o\{(1+3\nu) + 2(1+\nu)\,\ell n\,\rho\} - (1-\nu)a^2\sum_{m=0}^{M}\mu_{mo}\frac{m+1}{m+2}\rho^m\right] \tag{23}$$

$$M_{rt_o} = Q_{t_o} = 0 \tag{24}$$

$$Q_{r_o} = \frac{4D_o}{(1-\nu)a^3\rho} \tag{25}$$

$$V_o = Q_{r_o} \tag{26}$$

Next for n = 1, we have

$$\frac{\partial w_1}{\partial r} = \frac{1}{D(\nu-1)a}\left[A_1 + 3B_1\rho^2 - \frac{C_1}{\rho^2} + D_1(1 + \ell n\,\rho) + a^2\sum_{m=0}^{M}\mu_{m1}\frac{m+2}{(m+1)(m+3)}\rho^{m+1}\right]\cos\theta \tag{27}$$

$$\frac{\partial^2 w_1}{\partial r^2} = \frac{1}{D(\nu-1)a^2}\left[6B_1\rho + 2\frac{C_1}{\rho^3} + \frac{D_1}{\rho} + a^2\sum_{m=0}^{M}\mu_{m1}\frac{m+2}{m+3}\rho^m\right]\cos\theta \tag{28}$$

$$M_{r_1} = \frac{1}{(1-\nu)a^2}\left[2B_1(3+\nu)\rho + 2C_1\frac{1-\nu}{\rho^3} + D_1\frac{1+\nu}{\rho} - (1-\nu)a^2\sum_{m=0}^{M}\mu_{m1}\frac{\rho^m}{m+3}\right]\cos\theta \tag{29}$$

$$M_{t_1} = \frac{1}{(1-\nu)a^2}\left[2B_1(1+3\nu)\rho - 2C_1\frac{1-\nu}{\rho^3} + D_1\frac{1+\nu}{\rho} - (1-\nu)a^2\sum_{m=0}^{M}\mu_{m1}\frac{m+2}{m+3}\rho^m\right]\cos\theta \tag{30}$$

$$M_{rt_1} = \frac{1}{a^2}\left[2B_1\rho - \frac{2C_1}{\rho^3} + \frac{D_1}{\rho} + a^2\sum_{m=0}^{M}\mu_{m1}\frac{\rho^m}{m+3}\right]\sin\theta \tag{31}$$

$$Q_{r_1} = \frac{1}{(1-\nu)a^3}\left[8B_1 - \frac{2D_1}{\rho^2}\right]\cos\theta \tag{32}$$

$$Q_{t_1} = \frac{1}{(\nu-1)a^3}\left[8B_1 - \frac{2D_1}{\rho^2}\right]\sin\theta \tag{33}$$

$$V_1 = \frac{1}{(1-\nu)a^3}\left[2B_1(3+\nu) + 2C_1\frac{1-\nu}{\rho^4} - D_1\frac{3-\nu}{\rho^2} - (1-\nu)a^2\sum_{m=0}^{M}\mu_{m1}\frac{\rho^{m-1}}{m+3}\right]\cos\theta \tag{34}$$

Next for $n > 2$, when $n \neq m + 2$, we have

$$\frac{\partial w_n}{\partial r} = \frac{1}{D(\nu-1)a}\left[A_n n\rho^{n-1} + B_n(n+2)\rho^{n+1} - C_n n\rho^{-(n+1)} - D_n(n-2)\rho^{-(n-1)} + a^2\sum_{m=0}^{M}\mu_{mn}\frac{m+2}{(m+2)^2 - n^2}\rho^{m+1}\right]\cos n\theta \tag{35}$$

$$\frac{\partial^2 w_n}{\partial r^2} = \frac{1}{D(\nu-1)a^2}\left[A_n n(n-1)\rho^{n-2} + B_n(n+1)(n+2)\rho^n + C_n n(n+1)\rho^{-(n+2)} + D_n(n-1)(n-2)\rho^{-n} + a^2\sum_{m=0}^{M}\mu_{mn}\frac{(m+1)(m+2)}{(m+2)^2 - n^2}\rho^m\right]\cos n\theta \tag{36}$$

$$M_{r_n} = \frac{1}{(1-\nu)a^2}\left[A_n n(n-1)(1-\nu)\rho^{n-2} + B_n(n+1)\{(n+2) - \nu(n-2)\}\rho^n + C_n n(n+1)(1-\nu)\rho^{-(n+2)} + D_n(n-1)\{(n-2) - \nu(n+2)\}\rho^{-n} - (1-\nu)a^2\sum_{m=0}^{M}\mu_{mn}\frac{(m+2) - n^2}{(m+2)^2 - n^2}\rho^m\right]\cos n\theta \tag{37}$$

$$M_{t_n} = \frac{1}{(\nu-1)a^2}\left[A_n n(n-1)(1-\nu)\rho^{n-2} + B_n(n+1)\{(n-2) - \nu(n+2)\}\rho^n + C_n n(n+1)(1-\nu)\rho^{-(n+2)} + D_n(n-1)\{(n+2) - \nu(n-2)\}\rho^{-n} + (1-\nu)a^2\sum_{m=0}^{M}\mu_{mn}\frac{(m+1)(m+2)}{(m+2)^2 - n^2}\rho^m\right]\cos n\theta \tag{38}$$

$$M_{rt_n} = \frac{1}{a^2}\left[A_n n(n-1)\rho^{n-2} + B_n n(n+1)\rho^n - C_n n(n+1)\rho^{-(n+2)} - D_n n(n-1)\rho^{-n} + a^2\sum_{m=0}^{M}\mu_{mn}\frac{(m+1)n}{(m+2)^2 - n^2}\rho^m\right]\sin n\theta \tag{39}$$

$$Q_{r_n} = \frac{1}{(1-\nu)a^3}\left[4B_n n(n+1)\rho^{n-1} + 4D_n n(n-1)\rho^{-(n+1)}\right]\cos n\theta \tag{40}$$

$$Q_{t_n} = \frac{1}{(1-\nu)a^3}\left[4B_n n(n+1)\rho^{n-1} - 4D_n n(n-1)\rho^{-(n+1)}\right]\sin n\theta \tag{41}$$

$$V_n = \frac{n}{(\nu-1)a^3}\left[A_n n(n-1)(1-\nu)\rho^{n-3} - B_n(n+1)\{4 - n(1-\nu)\}\rho^{n-1} - C_n n(n+1)(1-\nu)\rho^{-(n+3)}\right.$$

$$\left. - D_n(n-1)\{4 + n(1-\nu)\}\rho^{-(n+1)} - (1-\nu)a^2\sum_{m=0}^{M}\mu_{mn}\frac{(m+1)n}{(m+2)^2 - n^2}\rho^{m-1}\right]\cos n\theta \tag{42}$$

Finally, for $n \geq 2$, when $n = m + 2$, the contribution of the particular integral, represented by the summation term with the symbol Σ, should be respectively replaced in Eq. (35) through (42) by the right hand side of the following formulas based on the particular integral (17).

$$\frac{\partial w_{pn}}{\partial r} = \frac{1}{D(\nu-1)a}\left[a^2\sum_{m=0}^{M}\mu_{mn}\frac{1 + (m+2)\ell n\rho}{2(m+2)}\rho^{m+1}\right]\cos n\theta \tag{43}$$

$$\frac{\partial^2 w_{pn}}{\partial r^2} = \frac{1}{D(\nu-1)a^2}\left[a^2\sum_{m=0}^{M}\mu_{mn}\frac{(m+1)(m+2)\ell n\rho + (2m+3)}{2(m+2)}\rho^{m}\right]\cos n\theta \tag{44}$$

$$M_{r_{pn}} = \frac{1}{(1-\nu)a^2}\left[\frac{(1-\nu)a^2}{2}\sum_{m=0}^{M}\mu_{mn}\left\{(m+1)\ell n\rho - \frac{1}{m+2}\right\}\rho^{m}\right]\cos n\theta \tag{45}$$

$$M_{t_{pn}} = \frac{1}{(\nu-1)a^2}\left[\frac{(1-\nu)a^2}{2}\sum_{m=0}^{M}\mu_{mn}\left\{(m+1)\ell n\rho + \frac{2m+3}{m+2}\right\}\rho^{m}\right]\cos n\theta \tag{46}$$

$$M_{rt_{pn}} = \frac{1}{a^2}\left[\frac{a^2}{2}\sum_{m=0}^{M}\mu_{mn}\{(m+1)\ell n\rho + 1\}\rho^{m}\right]\sin n\theta \tag{47}$$

$$Q_{r_{pn}} = Q_{t_{pn}} = 0 \tag{48}$$

$$V_{pn} = \frac{n}{(\nu-1)a^3}\left[\frac{(\nu-1)a^2}{2}\sum_{m=0}^{M}\mu_{mn}\{(m+1)\ell n\rho + 1\}\rho^{m-1}\right]\cos n\theta \tag{49}$$

Inner region ($\rho_b \leq \rho \leq \rho_c$): The expressions for deflection, slope, curvature and stress resultants for the inner region are obtained from those of the middle region, formulas (20) through (49), by replacing the constants of integrations A_o, B_o, ..., C_n, D_n with constants $\underline{A}_o$, $\underline{B}_o$, ..., $\underline{C}_n$, $\underline{D}_n$, respectively and denoting the deflection by $\underline{w}$ and stress resultants by $\underline{M}_r$, M_t, $\underline{M}_{rt}$, $\underline{Q}_r$, Q_t and $\underline{V}$, respectively.

Outer region ($\rho_d \leq \rho \leq 1$): Similar expressions for the outer region are obtained by using the constants $\overline{A}_o$, $\overline{B}_o$, ..., $\overline{C}_n$, $\overline{D}_n$ respectively in place of A_o, B_o, ..., C_n, D_n in formulas (20) through (49) and denoting the deflection by $\overline{w}$ and stress resultants by $\overline{M}_r$, $\overline{M}_t$, $\overline{M}_{rt}$, $\overline{Q}_r$, $\overline{Q}_t$, and $\overline{V}$, respectively.

Continuity conditions

The integration constants for the three regions are related by the conditions of continuity at the common boundaries between the regions, i.e. at $\rho = \rho_c$ and $\rho = \rho_d$. For continuity, we must have at these common boundaries,

$$\left[\ w\ \right]_{\rho_c} = \left[\underline{w}\ \right]_{\rho_c}, \qquad \left[\ w\ \right]_{\rho_d} = \left[\overline{w}\ \right]_{\rho_d} \tag{50}$$

$$\left[\frac{\partial w}{\partial r}\right]_{\rho_c} = \left[\frac{\partial \underline{w}}{\partial r}\right]_{\rho_c}, \qquad \left[\frac{\partial w}{\partial r}\right]_{\rho_d} = \left[\frac{\partial \overline{w}}{\partial r}\right]_{\rho_d} \tag{51}$$

$$\left[M_r\right]_{\rho_c} = \left[\underline{M}_r\right]_{\rho_c}, \qquad \left[M_r\right]_{\rho_d} = \left[\overline{M}_r\right]_{\rho_d} \tag{52}$$

$$\left[Q_r\right]_{\rho_c} = \left[\underline{Q}_r\right]_{\rho_c}, \qquad \left[Q_r\right]_{\rho_d} = \left[\overline{Q}_r\right]_{\rho_d} \tag{53}$$

By virtue of Eqs. (50 and (51), Eqs. (52) and (53) ensure the continuity of $\partial^2 w/\partial r^2$ and $\partial^3 w/\partial r^3$ at ρ_c and ρ_d. Hence, M_t and M_{rt} are also continuous at ρ_c and ρ_d. Substitutions of appropriate formulas from (20) through (49) into Eqs. (50) through (53) yield the required equations for solving the integration constants of the unheated inner and outer regions in terms of those of heated middle region. The results are as follows:

Inner region ($\rho_b \le \rho \le \rho_c$): First, for n = 0, we get

$$\underline{A}_0 = A_0 + a^2 \sum_{m=0}^{M} \mu_{mo} \frac{1 - (m+2)\,\ell n\,\rho_c}{(m+2)^2}\,\rho_c^{m+2} \tag{54}$$

$$\underline{C}_o = C_o + a^2 \sum_{m=0}^{M} \mu_{mo} \frac{\rho_c^{m+2}}{m+2} \tag{55}$$

Next, for $n \ge 1$, when $n \ne m + 2$, we obtain

$$\underline{A}_n = A_n + a^2 \sum_{m=0}^{M} \mu_{mn} \frac{\rho_c^{m+2-n}}{2n(m+2-n)} \tag{56}$$

and for $n \ge 2$, when $n = m + 2$, we get

$$\underline{A}_n = A_n + a^2 \sum_{m=0}^{M} \mu_{mn}\left[2\,\ell n\,\rho_c + \frac{1}{m+2}\right] \frac{1}{4(m+2)} \tag{57}$$

Next, for all values of $n \ge 1$, we get

$$\underline{C}_n = C_n - a^2 \sum_{m=0}^{M} \mu_{mn} \frac{\rho_c^{m+2+n}}{2n(m+2+n)} \tag{58}$$

Finally, for all values of $n \ge 0$, we obtain

$$\underline{B}_n = B_n \tag{59}$$

$$\underline{D}_n = D_n \tag{60}$$

Outer region ($\rho_d \le \rho \le 1$): The integration constants of the outer region are obtained from formulas (54) through (60) by replacing ρ_c with ρ_d and constants $\underline{A}_o, \underline{B}_o, \ldots, \underline{C}_n, \underline{D}_n$ with constants $\overline{A}_o, \overline{B}_o, \ldots, \overline{C}_n, \overline{D}_n$, respectively.

Having solved for the integration constants of the unheated inner and outer regions in terms of those of the heated middle region, it now remains to determine the integration constants of the heated region. This is accomplished by applying the boundary conditions.

Boundary conditions

Both the outer and innter boundaries are free. Therefore,

$$\left[M_r\right]_{\rho = 1} = 0 \tag{61}$$

$$\left[M_r\right]_{\rho = \rho_b} = 0 \tag{62}$$

$$\left[V\right]_{\rho = 1} = 0 \tag{63}$$

$$\left[V\right]_{\rho = \rho_b} = 0 \tag{64}$$

Substitutions of appropriate formulas from (20) through (49) into the boundary conditions (61) through (64) and elimination of the integration constants of the inner unheated region from the resulting equations by means of formulas (54) through (60) and the corresponding formulas for the outer unheated region yield the required equations for determining the integration constants of the middle heated region.

First, for n = 0, we have by solving Eqs. (61) through (63)

$$B_o = \frac{(1-\nu)a^2}{2(1+\nu)(1-\rho_b^2)} \sum_{m=0}^{M} \mu_{m0} \frac{\rho_d^{m+2} - \rho_c^{m+2}}{m+2} \tag{65}$$

$$C_o = \frac{1}{1-\rho_b^2} \sum_{m=0}^{M} \mu_{mo} \frac{\rho_d^{m+2}\rho_b^2 - \rho_c^{m+2}}{m+2} \tag{66}$$

$$D_o = 0 \tag{67}$$

By virtue of (67), Eq. (64) is identically satisfied. The constant A_o is determined from the condition that the deflection vanishes at the three support points, where $\rho = \rho_s$. Therefore,

$$A_o = a^2 \sum_{m=0}^{M} \mu_{mn} \frac{(m+2)(\ell n\, \rho_c - \ell n\, \rho_s) - 1}{(m+2)^2} \rho_c^{m+2} - B_o\rho_s^2 - C_o \ell n\, \rho_s , \qquad \text{if } \rho_b \le \rho_s \le \rho_c \tag{68}$$

$$A_o = -a^2 \sum_{m=0}^{M} \mu_{mn} \frac{\rho_s^{m+2}}{(m+2)^2} - B_o\rho_s^2 - C_o \ell n\, \rho_s , \qquad \text{if } \rho_c \le \rho_s \le \rho_d \tag{69}$$

$$A_o = a^2 \sum_{m=0}^{M} \mu_{mn} \frac{(m+2)(\ell n\, \rho_d - \ell n\, \rho_s) - 1}{(m+2)^2} \rho_d^{m+2} - B_o\rho_s^2 - C_o \ell n\, \rho_s , \qquad \text{if } \rho_d \le \rho_s \le 1 \tag{70}$$

Similarly, for n = 1, we have by solving Eqs. (61) through (63),

$$B_1 = \frac{a^2(1-\nu)}{2(3+\nu)(1-\rho_b^4)} \sum_{m=0}^{M} \mu_{m1} \frac{\rho_d^{m+3} - \rho_c^{m+3}}{m+3} \tag{71}$$

$$C_1 = \frac{a^2}{2(\rho_b^4 - 1)} \sum_{m=0}^{M} \mu_{m1} \frac{\rho_d^{m+3}\rho_b^4 - \rho_c^{m+3}}{m+3} \tag{72}$$

$$D_1 = 0 \tag{73}$$

Using this solution for B_1, C_1 and D_1, it can be shown that Eq. (64) is satisfied. For obtaining the constant A_o, we apply the condition of zero deflection at the three support points. This gives

$$A_1 = \frac{a^2}{2\rho_s^2} \sum_{m=0}^{M} \mu_{m1} \left[\frac{\rho_c^2}{m+3} - \frac{\rho_s^2}{m+1} \right] \rho_c^{m+1} - B_1\rho_s^2 - C_1/\rho_s^2 , \quad \text{if } \rho_b \le \rho_s \le \rho_c \tag{74}$$

$$A_1 = -a^2 \sum_{m=0}^{M} \mu_{m1} \frac{\rho_s^{m+1}}{(m+1)(m+3)} - B_1\rho_s^2 - C_1/\rho_s^2 , \quad \text{if } \rho_c \le \rho_s \le \rho_d \tag{75}$$

$$A_1 = \frac{a^2}{2\rho_s^2} \sum_{m=0}^{M} \mu_{m1} \left[\frac{\rho_d^2}{m+3} - \frac{\rho_s^2}{m+1} \right] \rho_d^{m+1} - B_1\rho_s^2 - C_1/\rho_s^2, \quad \text{if } \rho_d \le \rho_s \le 1 \tag{76}$$

Next, for $n \ge 2$, when $n \ne m+2$, the boundary conditions (61) through (64) yield the following four equations after performing some algebraic manipulations.

$$\frac{1-\nu}{3+\nu}(n-1)\left(1 - \rho_b^{2n}\right) A_n + \frac{n^2(1-\nu)^2 + 8(1+\nu)}{n(1-\nu)(3+\nu)}\left(1 - \rho_b^{2n+2}\right) B_n$$

$$= \frac{1-\nu}{3+\nu}(n-1)a^2 \sum_{m=0}^{M} \mu_{mn} \frac{\rho_b^{2n}\,\rho_c^{m+2-n} - \rho_d^{m+2-n}}{2n(m+2-n)} + a^2 \sum_{m=0}^{M} \mu_{mn} \frac{\rho_d^{m+2+n} - \rho_c^{m+2+n}}{2n(m+2+n)} \tag{77}$$

$$n\left(1 - \rho_b^{2n-2}\right)A_n + (n+1)\left(1 - \rho_b^{2n}\right)B_n = a^2 \sum_{m=0}^{M} \mu_{mn} \frac{\rho_b^{2n-2}\,\rho_c^{m+2-n} - \rho_d^{m+2-n}}{2(m+2-n)} \tag{78}$$

$$C_n = -\frac{1-\nu}{3+\nu}(n-1)\,A_n - \frac{n^2(1-\nu)^2 + 8(1+\nu)}{n(1-\nu)(3+\nu)} B_n - \frac{1-\nu}{3+\nu}(n-1)\,a^2 \sum_{m=0}^{M} \mu_{mn} \frac{\rho_d^{m+2-n}}{2n(m+2-n)} + a^2 \sum_{m=0}^{M} \mu_{mn} \frac{\rho_d^{m+2+n}}{2n(m+2+n)} \tag{79}$$

$$D_n = \frac{1-\nu}{3+\nu}\left[nA_n + (n+1)B_n + a^2 \sum_{m=0}^{M} \mu_{mn} \frac{\rho_d^{m+2-n}}{2(m+2-n)} \right] \tag{80}$$

A_n and B_n can be obtained by solving Eqs. (77) and (78). Then C_n and D_n can be evaluated from formulas (79) and (80).

Finally, for $n \ge 2$, when $n = m+2$, Eqs. (77) through (80) remain valid, if the following replacements are made.

$$\frac{1 + 2(m+2)\,\ell n\,\rho_c}{4\,(m+2)^2} \quad \text{for} \quad \frac{\rho_c^{m+2-n}}{2n(m+2-n)} \tag{81}$$

$$\frac{1 + 2(m+2)\,\ell n\,\rho_d}{4(m+2)^2} \quad \text{for} \quad \frac{\rho_d^{m+2-n}}{2n(m+2-n)} \tag{82}$$

Support deflection

For $n > 2$, the datum plane for deflection measurement is not yet defined. Let δ_1, δ_2 and δ_3 be the respective support point deflections obtained from the above analysis for all $n \geq 2$. Further, let

$$\delta_{av} = (\delta_1 + \delta_2 + \delta_3)/3 \tag{83}$$

$$\theta_x = (\delta_2 - \delta_3)/2s \sin 60^\circ = (\delta_2 - \delta_3)/\sqrt{3}s \tag{84}$$

$$\theta_y = \left[(\delta_2 + \delta_3)/2 - \delta_1\right] /(s + s\cos 60^\circ) = (\delta_2 + \delta_3 - 2\delta_1)/3s \tag{85}$$

Then from the deflection of every point (x,y) the following quantity must be subtracted.

$$\delta_{sup} = \delta_{av} + y\theta_x - x\theta_y \tag{86}$$

This will establish the plane of three support points as the datum plane for deflection.

Numerical verification

With the establishment of the datum plane for deflection in the preceeding section, the formal solution of the circular flat plate boundary value problem for non-symmetric thermal bowing is completed. The solution was implemented in a computer software for the convenience of making rapid calculations. In order to verify the software, a series of test cases were run and compared with Nastran based finite element analysis.

For the numerical test runs, the flat mirror was assumed to be made of six sectorial panels fused together along their straight edges as shown in Figure 4. The panels were assumed to be made of the same material but with different spatially averaged coefficients of thermal expansion, resulting in different thermal moments, when subjected to temperature gradients through the mirror thickness. The assumed relative azimuthal variation of applied thermal moments is shown in Figure 4. It was further assumed to vary the thermal moment in each panel radially such that the integrated value of the moment over the area of that panel remained invariant regardless of the radial variation, which is given by $\mu_{mn}\rho^m$. The integrated thermal moment over a panel is

$$\frac{2\pi}{6}\int_{\rho_c}^{\rho_d} (\mu_{mn}\rho^m)\,\rho\,d\rho = \frac{\pi}{3}\mu_{mn}\frac{\rho_d^{m+2} - \rho_c^{m+2}}{m+2}$$

When $m = 0$, this gives $\pi\mu_{on}(\rho_d^2 - \rho_c^2)/6$. Therefore, by virtue of the invariance assumption, we have

$$\frac{\pi}{3}\mu_{mn}\frac{\rho_d^{m+2} - \rho_c^{m+2}}{m+2} = \frac{\pi}{6}\mu_{on}(\rho_d^2 - \rho_c^2)$$

Therefore,

$$\mu_{mn} = \frac{(m+2)(\rho_d^2 - \rho_c^2)}{2(\rho_d^{m+2} - \rho_c^{m+2})}\mu_{on} \tag{87}$$

For any given value of $m = 0$, the radial variation for any non-zero value of m ($m \geq 1$) was assumed to be given by Eq. (87).

The assumed azimuthal step-function type variation of the thermal moment shown with relative values in Figure 4 was decomposed into Fourier components involving both cos nθ and sin nθ terms up to a maximum of N = 12 for each. Four cases of radial variation combined with this azimuthal variation were considered: In a given sector, (a) radially uniform with m = 0, (b) radially linear with m = 1, (c) radially parabolic with m = 2, and (d) radially cubic with m = 3. The test mirror for analytical correlation had the following geometric and material characteristics: a = outer radius = 50 inches; b = central hole = 0 or 10 inches; D = flexural rigidity = 1.34×10^7 lb-in; E = Young's modulus = 10^7 psi; ν = Poisson's ratio = 0.17. The analytical results are plotted in Figure 5. These plots demonstrate a consistently excellent correlation between the closed form and Nastran solutions. Many more test cases[2] were run and the correlation between the two methods was always found to be excellent.

Applications

Normalized performance curves

The closed form solution and the associated computer software were utilized to generate normalized performance curves. The thermal bowing due to an applied thermal moment is directly proportional to the thermal moment and the square of the circular plate outer radius, and is inversely proportional to the Young's modulus and the bending moment of inertia of the plate cross section per unit width. Hence, for a given m and n,

$$\text{Normalized deflection} = (EI/a^2\mu_{mn})w \tag{88}$$

for the cosine series of the thermal moment. For the sine series, the normalized deflection is obtained by replacing μ_{mn} with ξ_{mn} in Eq. (88). For the normalized rms deflection, it does not matter whether the thermal moment is of the cosine series type or of the sine series type. For a given m and n,

$$\begin{aligned}\text{Normalized rms deflection} &= (EI/a^2\mu_{mn})w_{rms} \\ &= (EI/a^2\xi_{mn})w_{rms}\end{aligned} \tag{89}$$

Since the (engineering) unit for μ_{mn} and ξ_{mn} is lb-in/in and that for I is in^4/in, the normalized rms reflection is non-dimensional.

For the performance curves, two modifications were made in the normalized rms deflection. Since tilt does not affect the optical surface quality of a mirror, both components of tilt were taken out from the deflection data before computing the rms value of the residual deflection. The resulting normalized rms figure error was then divided, for convenience, by the wavelength $\lambda = 24.91 \times 10^{-6}$ inch (6328 Å in the visible light spectrum). All the performance curve plots have been prepared for the normalized rms figure error divided by λ .

These performance curves for thermal bowing were prepared[2] for flat circular optical elements with normalized central hole radius ρ_b = 0, 0.1, 0.2 and 0.3. Further, for each of these values ρ_b, several different values of Poisson's ratio, typical of some common mirror materials were chosen: ν = 0 for beryllium (actual value 0.03), 0.17 for ULE and fused silica, 0.24 for Zerodur and 0.30. Metals like invar, steel, aluminum, titanium and molybdenum are more or less covered by these choices of ν .

Some illustrative performance curves are presented in Figure 6 for flat circular mirros with a normalized central hole radius ρ_b = 0.2. In viewing these performance curves, it may be recalled that the deflection functions for n = 0, n = 1 and n ≥ 2 are all different, yielding three different families of curves. Those for n ≥ 2 are all parallel and give, for a given value of m, decreasing values of the normalized rms figure error with increasing n. They also intersect the curves for n = 0 and n = 1.

The effect of Poisson's ratio on the normalized rms figure is mostly moderate. It is observed that

- For m = n = 0, the Poisson's ratio has no effect on the normalized rms figure error
- For n = 0 and m > 0, the normalized rms figure error decreases with increase in the Poisson's ratio
- For n > 0 with m ≥ 0, this effect is reversed. The normalized rms figure error increases with increase in the Poisson's ratio.

The performance curves of Figure 6 are also applicable for the sin nθ terms of the thermal moment given by Eq. (7) (except for n = 0, because sin nθ = 0 in that case), if μ_{mn} is replaced by ξ_{mn}. Additionally, the locations of the three support points have no effect either on the performance curves or on the rms figure error because of the kinematic nature of the 3-point support concept.

Coherent superposition of thermal bowing components

The performance curves of Figure 6 may be used to make a first approximation of the resultant rms figure error due to more than one thermal moment terms in Eq. (7) by taking the rss or the square root of the sum of the squares of the rms figure errors due to individual terms in accordance with the common optical/system engineering practice in the preliminary stages of a design. This practice is based on the assumption that the constituent figure errors are orthogonal to each other. If this assumption is not satisfied sufficiently, the rms approximation may be crude and in need of a modification. With this modification the true rms value may be obtained from[2]

$$\begin{aligned}w_{rms}^2 &= \sum_{j=1}^{J} c_j^2 w_{rms_j}^2 \\ &\quad + \sum_{j=1}^{J} \sum_{k=1}^{j-1} \kappa_{jk} c_j c_k w_{rms_j} w_{rms_k}\end{aligned} \tag{90}$$

where κ_{jk} may be called the "coherent superposition coefficient" given by

$$\kappa_{jk} = \frac{\sum_i 2\,\beta_i a_{ij} a_{ik}}{w_{rms_j}\, w_{rms_k} \sum_i \beta_i} \tag{91}$$

Various quantities used in expressions (90) and (91) are defined as follows.

J = (M+1)(N+1) + (M+1)N = total number of terms used for M_T (cosine terms + sine terms)

β_i = weight factor associated with point "i" on the mirror

j = thermal moment term number (for a given m and n)

a_{ij} = figure error at point "i" due to the unit valued "j" term of the thermal moment function

c_j = thermal moment coefficient for the "j" term (i.e. either μ_{mn} or ξ_{mn})

w_{rms_j} = rms figure error due to the "j" term of thermal moment function

κ_{jk} = coherent superposition coefficient for combined figure error due to unit thermal moment values for the "j" and "k" terms

The first term on the right side of Eq. (90) represents the sum of the squares of the rms figure error due to individual terms of the thermal moment. Therefore, in order for the rss to be the first approximation of the resultant rms figure error, the second term on the right side of Eq. (90) must be acceptably small. The second term actually vanishes if the figure error functions due to "j" and "k" terms are orthogonal. Otherwise, the second term must be included.

The coherent superposition coefficient κ_{jk} is, in general, bounded by ± 2, i.e., $-2 \leq \kappa_{jk} \leq 2$. In our case, it is zero, except when $n_j = n$ and $n_k = n$ in the j-th and k-th terms, respectively ; i.e.

$$\left.\begin{aligned} w_j(\rho) \cos n_j\theta &= w_j(\rho) \cos n\theta \\ w_k(\rho) \cos n_k\theta &= w_k(\rho) \cos n\theta \end{aligned}\right\} \qquad (92)$$

where $w_j(\rho)$ and $w_k(\rho)$ are functions of ρ. The same is true for the sine terms. It is seen from the illustrative Table 2 that the non-zero values of κ_{jk} are all very nearly equal to 2 near the diagonal of each sub-matrix, and they more or less decrease gradually with increase in distance from the diagonal. The smallest value in the table is 1.78 for $m_j = 0$, $m_k = 9$ and $n = 0$.

Curved Circular Mirrors

The analytical approach of this paper is applicable to the nonsymmetric thermal bowing of curved circular mirrors, the elastic deformation of which is governed by E. Reissner's shallow spherical shell (f/number ≥ 0.4) equations.[3,4] This work has been performed by the present author and will be published in the near future. Some illustrative examples of the results obtained are shown in the mirror deflection plots of Figure 7, which correlates the curved mirror closed form solution with Nastran based finite element analysis for the test run thermal moment loading shown in Figure 4. The correlation is once again excellent. A variety of additional test runs were made, and they all demonstrated equally good correlation between the two methods.

Concluding Remarks

The normalized performance curves together with the coherent superposition coefficients provide us with a useful, efficient and accurate means of determining the thermal bowing figure error for flat circular mirrors subjected to nonuniform thermal moment loadings. For cases outside the framework of the performance curve, the closed form solution can be used. With all the required equations available in this paper, it is relatively simple to develop a computer software for the convenience of making rapid calculations. Such a software is extremely economic in comparison with a two-dimensional finite element model and is equally accurate.

The closed form solution is applicable to lightweighted mirrors of both sandwich and open back constructions by taking the cross sectional moment of inertia with respect to the neutral surface of the mirror in the calculation of flexural rigidity. The effect of the slight deviation from isotropy due to the lightweighted rib pattern is relatively small. Further, since the support reactions are zero due to the kinematic nature of the mirror mounts, the transverse shear deflection can only be due to non-uniform distribution of thermal moment, and that happens to be relatively small or zero. In any event, the transverse shear deflection can be added on by considering the radial and tangential components of the transverse shear force, performing some mathematical manipulations and computing the shear deflection as in the case of beams.

The analytical approach of this paper is also applicable to non-uniform thermal bowing of curved circular mirrors, which are governed by E. Reissner's shallow spherical shell equations. Further, the analytical expression used to represent the thermal moment distribution can be used to construct a variety of non-uniform distributions.

This paper hopefully demonstrates to some extent a viewpoint that in this age of ever-increasing FEM technology, the classical methods of engineering mechanics still have a very useful and much needed role to play in opto-structural engineering.

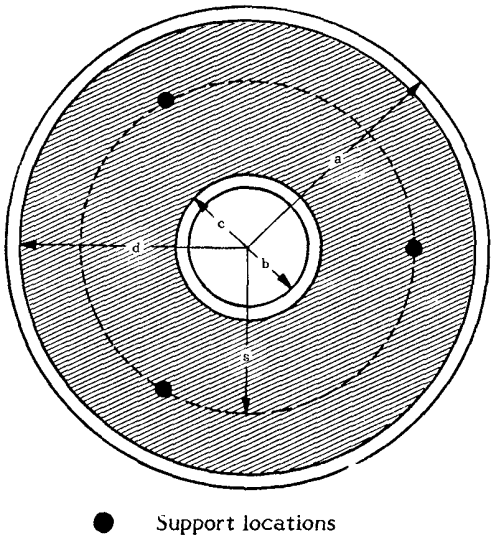

● Support locations

Heated region:	Support circle radius:
$c \leq r \leq d$, where	$r = s$, where
$b \leq c \leq d \leq a$	$b \leq s \leq a$

Figure 1. Geometry of heated aperture and kinematic support locations

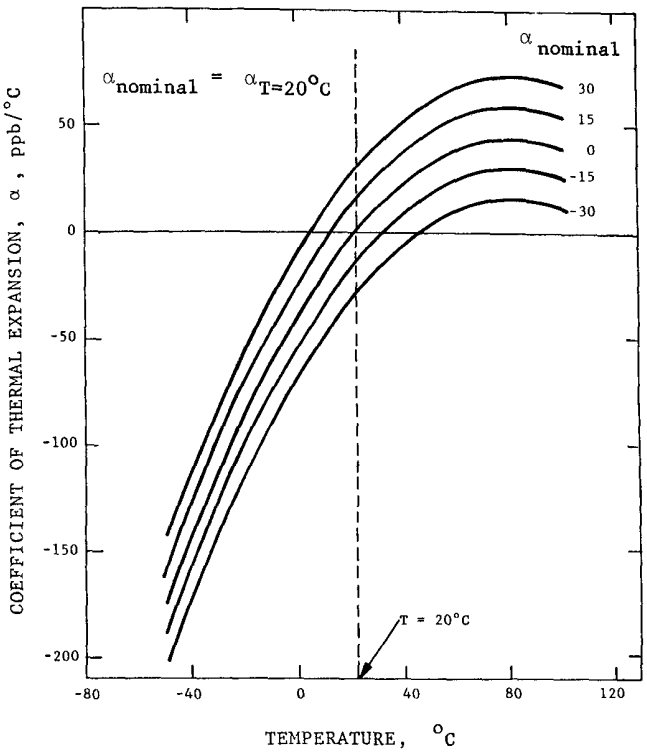

Figure 2. Temperature variation of ULE coefficient of thermal expansion

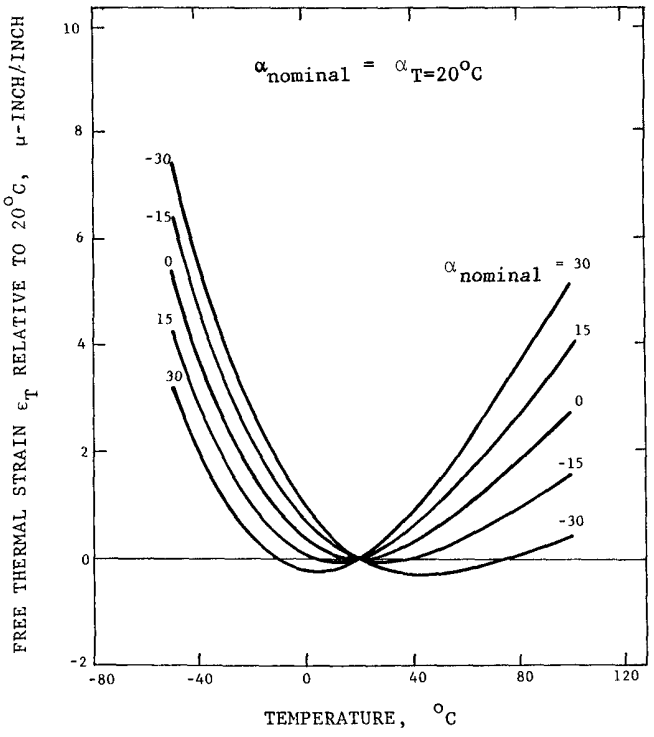

Figure 3. Temperature variation of free thermal strain ε_T in ULE based on 20°C reference temperature.

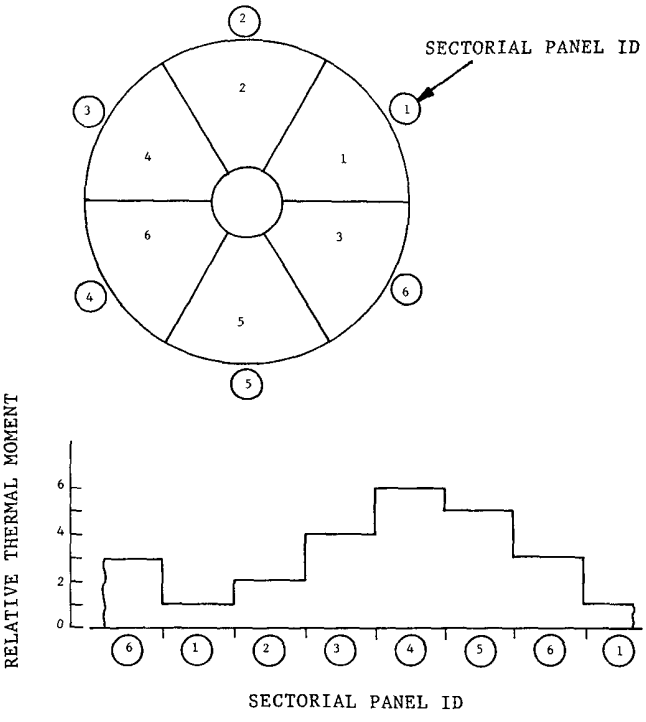

Figure 4. Relative azimuthal distribution of applied thermal moment in test runs for correlation with Nastran based finite element analysis.

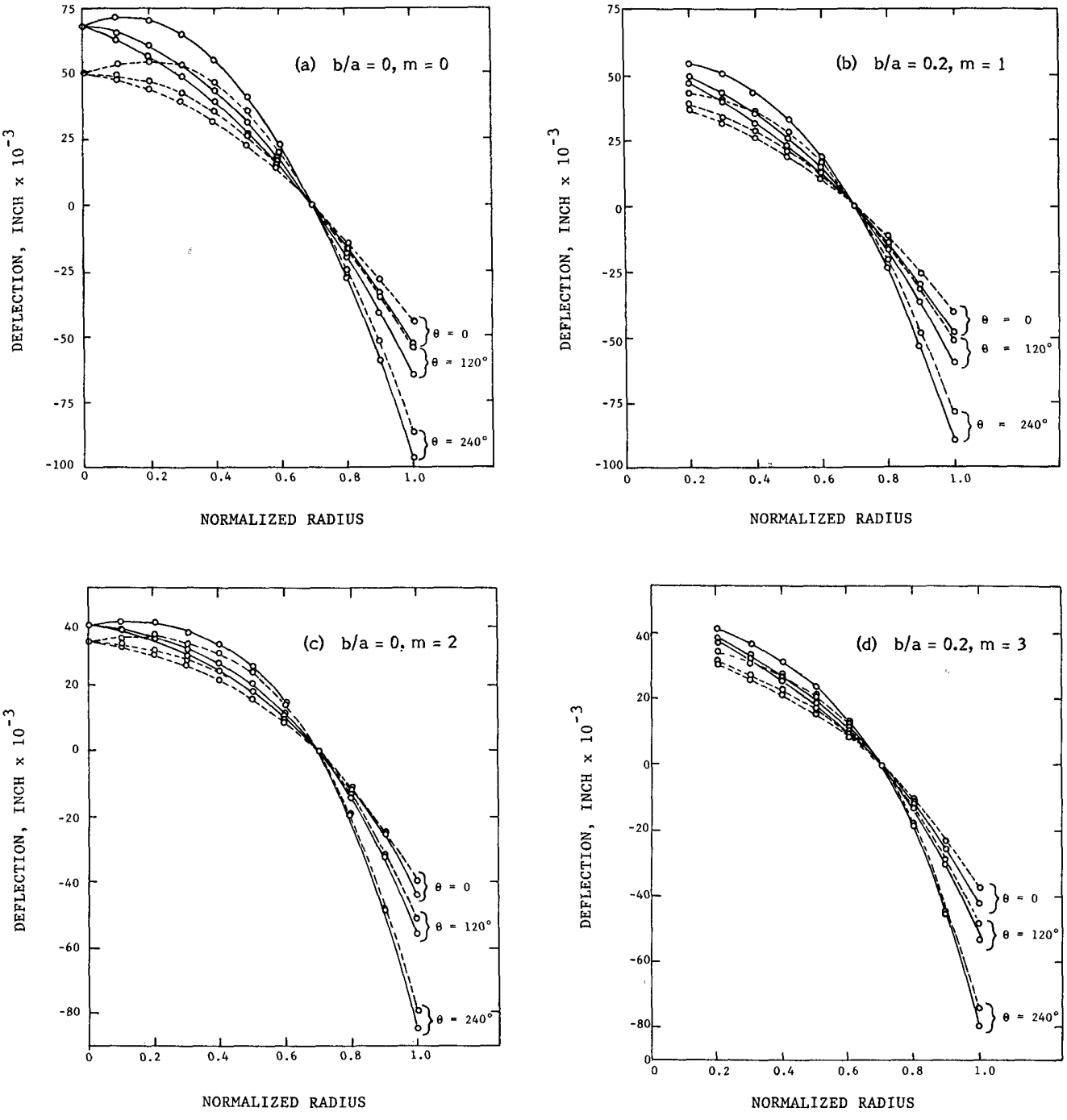

Figure 5. Test run correlation between Nastran and closed form solutions for a flat circular mirror subjected to the thermal moment distribution of Figure 4.

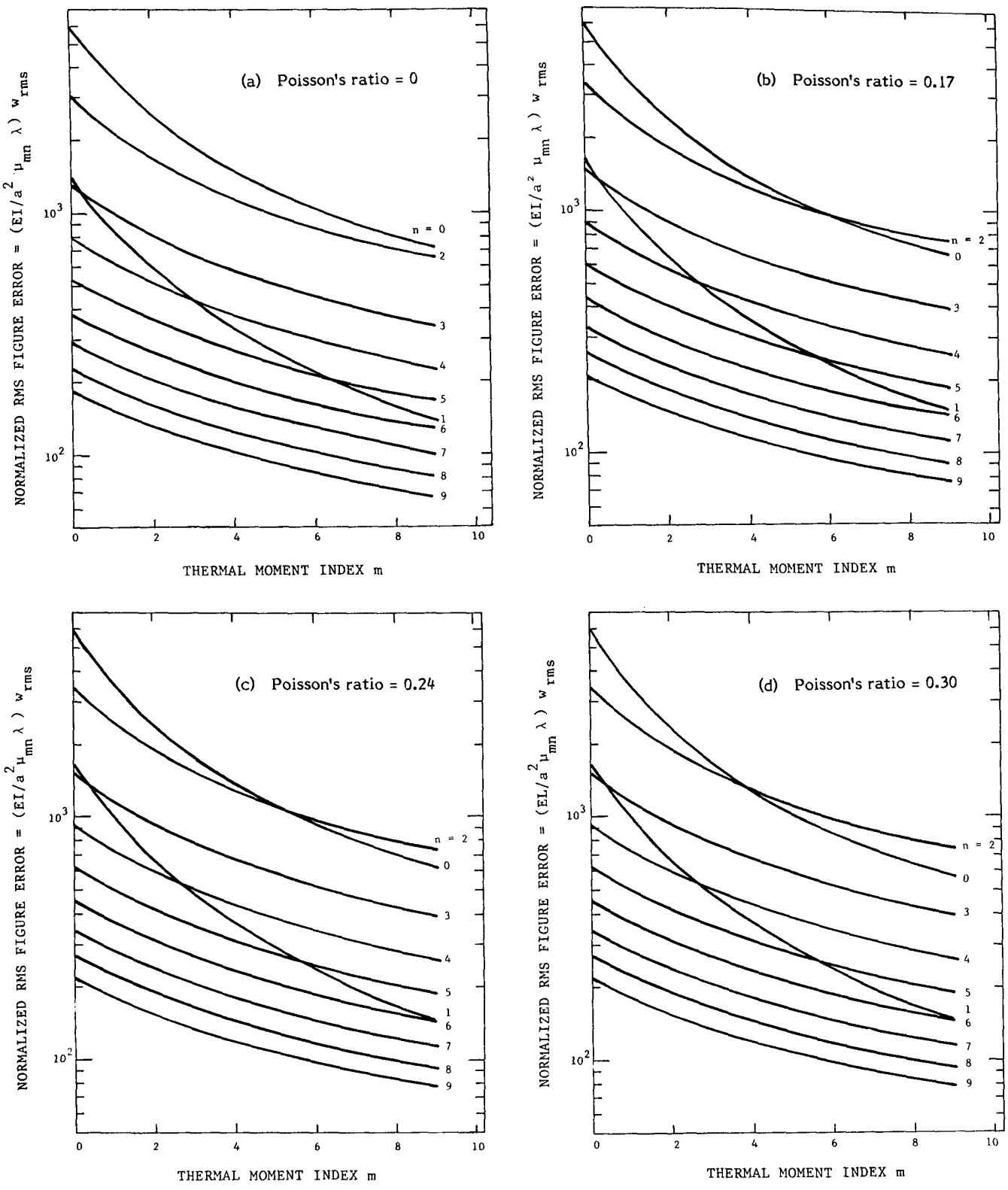

λ = 24.91 micro-inches (6328 Å)

Figure 6. Variation of normalized rms figure error with radial index m and azimuthal index n of thermal moment distribution, when the normalized central hole radius of a flat circular mirror is 0.2.

Table 2. Coherent superposition coefficients for b/a = 0.2 and ν = 0.17

n	m_j	m_k = 0	1	2	3	4	5	6	7	8	9
0	0	2 0	1 99802	1 99464	1 99197	1 99038	1 98966	1 98952	1 98973	1 99012	1 99061
	1	1 99802	2 0	1 99914	1 99781	1 99677	1 99613	1 99577	1 99562	1 99558	1 99560
	2	1 99464	1 99914	2 0	1 99967	1 99913	1 99866	1 99828	1 99797	1 99771	1 99748
	3	1 99197	1 99781	1 99967	2 0	1 99986	1 99959	1 99928	1 99897	1 99864	1 99832
	4	1 99038	1 99677	1 99913	1 99986	2 0	1 99992	1 99973	1 99948	1 99918	1 99886
	5	1 98966	1 99613	1 99866	1 99959	1 99992	2 0	1 99994	1 99979	1 99956	1 99928
	6	1 98952	1 99577	1 99828	1 99928	1 99973	1 99994	2 0	1 99995	1 99981	1 99961
	7	1 98973	1 99562	1 99797	1 99897	1 99948	1 99979	1 99995	2 0	1 99996	1 99983
	8	1 99012	1 99558	1 99771	1 99864	1 99918	1 99956	1 99981	1 99996	2 0	1 99996
	9	1 99061	1 99560	1 99748	1 99832	1 99886	1 99928	1 99961	1 99983	1 99996	2 0
1	0	2 0	1 98952	1 96777	1 94447	1 92383	1 90709	1 89391	1 88424	1 87682	1 87096
	1	1 98952	2 0	1 99389	1 98154	1 96829	1 95639	1 94626	1 93846	1 93209	1 92695
	2	1 96777	1 99389	2 0	1 99659	1 98966	1 98211	1 97491	1 96901	1 96386	1 95955
	3	1 94447	1 98154	1 99659	2 0	1 99809	1 99413	1 98949	1 98532	1 98137	1 97790
	4	1 92383	1 96829	1 98966	1 99809	2 0	1 99890	1 99638	1 99369	1 99083	1 98812
	5	1 90709	1 95639	1 98211	1 99413	1 99890	2 0	1 99917	1 99771	1 99578	1 99375
	6	1 89391	1 94626	1 97491	1 98949	1 99638	1 99917	2 0	1 99954	1 99840	1 99695
	7	1 88424	1 93846	1 96901	1 98532	1 99369	1 99771	1 99954	2 0	1 99949	1 99851
	8	1 87682	1 93209	1 96386	1 98137	1 99083	1 99578	1 99840	1 99949	2 0	1 99942
	9	1 87096	1 92695	1 95955	1 97790	1 98812	1 99375	1 99695	1 99851	1 99942	2 0
2	0	2 0	1 99723	1 99161	1 98558	1 98006	1 97521	1 97122	1 96773	1 96480	1 96230
	1	1 99723	2 0	1 99844	1 99526	1 99175	1 98836	1 98540	1 98271	1 98039	1 97835
	2	1 99161	1 99844	2 0	1 99912	1 99729	1 99517	1 99313	1 99118	1 98942	1 98784
	3	1 98558	1 99526	1 99912	2 0	1 99949	1 99838	1 99710	1 99576	1 99448	1 99328
	4	1 98006	1 99175	1 99729	1 99949	2 0	1 99968	1 99901	1 99816	1 99728	1 99640
	5	1 97521	1 98836	1 99517	1 99838	1 99968	2 0	1 99980	1 99936	1 99880	1 99819
	6	1 97122	1 98540	1 99313	1 99710	1 99901	1 99980	2 0	1 99986	1 99956	1 99916
	7	1 96773	1 98271	1 99118	1 99576	1 99816	1 99936	1 99986	2 0	1 99991	1 99970
	8	1 96480	1 98039	1 98942	1 99448	1 99728	1 99880	1 99956	1 99991	2 0	1 99994
	9	1 96230	1 97835	1 98784	1 99328	1 99640	1 99819	1 99916	1 99970	1 99994	2 0
3	0	2 0	1 99234	1 97830	1 96402	1 95091	1 94019	1 93024	1 92325	1 91595	1 91030
	1	1 99234	2 0	1 99632	1 98914	1 98112	1 97391	1 96675	1 96160	1 95596	1 95158
	2	1 97830	1 99632	2 0	1 99807	1 99394	1 98950	1 98460	1 98093	1 97671	1 97338
	3	1 96402	1 98914	1 99807	2 0	1 99883	1 99651	1 99341	1 99092	1 98786	1 98536
	4	1 95091	1 98112	1 99394	1 99883	2 0	1 99935	1 99770	1 99617	1 99406	1 99224
	5	1 94019	1 97391	1 98950	1 99651	1 99935	2 0	1 99948	1 99865	1 99730	1 99602
	6	1 93024	1 96675	1 98460	1 99341	1 99770	1 99948	2 0	1 99971	1 99910	1 99829
	7	1 92325	1 96160	1 98093	1 99092	1 99617	1 99865	1 99971	2 0	1 99973	1 99922
	8	1 91595	1 95596	1 97671	1 98786	1 99406	1 99730	1 99910	1 99973	2 0	1 99982
	9	1 91030	1 95158	1 97338	1 98536	1 99224	1 99602	1 99829	1 99922	1 99982	2 0
4	0	2 0	1 98992	1 97153	1 95256	1 93489	1 92038	1 90723	1 89615	1 88601	1 87770
	1	1 98992	2 0	1 99519	1 98562	1 97474	1 96493	1 95549	1 94715	1 93926	1 93264
	2	1 97153	1 99519	2 0	1 99740	1 99174	1 98562	1 97916	1 97309	1 96711	1 96194
	3	1 95256	1 98562	1 99740	2 0	1 99837	1 99516	1 99108	1 98687	1 98248	1 97854
	4	1 93489	1 97474	1 99174	1 99837	2 0	1 99906	1 99696	1 99431	1 99125	1 98836
	5	1 92038	1 96493	1 98562	1 99516	1 99906	2 0	1 99934	1 99788	1 99585	1 99377
	6	1 90723	1 95549	1 97916	1 99108	1 99696	1 99934	2 0	1 99957	1 99844	1 99709
	7	1 89615	1 94715	1 97309	1 98687	1 99431	1 99788	1 99957	2 0	1 99961	1 99886
	8	1 88601	1 93926	1 96711	1 98248	1 99125	1 99585	1 99844	1 99961	2 0	1 99978
	9	1 87770	1 93264	1 96194	1 97854	1 98836	1 99377	1 99709	1 99886	1 99978	2 0
5	0	2 0	1 98860	1 96696	1 94484	1 92507	1 90517	1 88948	1 87621	1 86412	1 85351
	1	1 98860	2 0	1 99415	1 98269	1 97035	1 95667	1 94512	1 93473	1 92518	1 91658
	2	1 96696	1 99415	2 0	1 99680	1 99040	1 98183	1 97382	1 96609	1 95880	1 95204
	3	1 94484	1 98269	1 99680	2 0	1 99808	1 99370	1 98863	1 98321	1 97785	1 97269
	4	1 92507	1 97035	1 99040	1 99808	2 0	1 99845	1 99561	1 99197	1 98809	1 98416
	5	1 90517	1 95667	1 98183	1 99370	1 99845	2 0	1 99920	1 99723	1 99476	1 99201
	6	1 88948	1 94512	1 97382	1 98863	1 99561	1 99920	2 0	1 99935	1 99801	1 99621
	7	1 87621	1 93473	1 96609	1 98321	1 99197	1 99723	1 99935	2 0	1 99959	1 99859
	8	1 86412	1 92518	1 95880	1 97785	1 98809	1 99476	1 99801	1 99959	2 0	1 99970
	9	1 85351	1 91658	1 95204	1 97269	1 98416	1 99201	1 99621	1 99859	1 99970	2 0
6	0	2 0	1 98747	1 96375	1 93843	1 91463	1 89322	1 87431	1 85770	1 84314	1 83034
	1	1 98747	2 0	1 99363	1 98056	1 96561	1 95075	1 93679	1 92398	1 91238	1 90193
	2	1 96375	1 99363	2 0	1 99638	1 98853	1 97910	1 96935	1 95986	1 95092	1 94262
	3	1 93843	1 98056	1 99638	2 0	1 99777	1 99275	1 98650	1 97982	1 97316	1 96673
	4	1 91463	1 96561	1 98853	1 99777	2 0	1 99855	1 99518	1 99085	1 98614	1 98132
	5	1 89322	1 95075	1 97910	1 99275	1 99855	2 0	1 99902	1 99666	1 99358	1 99014
	6	1 87431	1 93679	1 96935	1 98650	1 99518	1 99902	2 0	1 99930	1 99762	1 99536
	7	1 85770	1 92398	1 95986	1 97982	1 99085	1 99666	1 99930	2 0	1 99949	1 99824
	8	1 84314	1 91238	1 95092	1 97316	1 98614	1 99358	1 99762	1 99949	2 0	1 99963
	9	1 83034	1 90193	1 94262	1 96673	1 98132	1 99014	1 99536	1 99824	1 99963	2 0
7	0	2 0	1 98650	1 95979	1 93330	1 90641	1 88176	1 86052	1 83982	1 82601	1 81174
	1	1 98650	2 0	1 99249	1 97869	1 96171	1 94450	1 92862	1 91274	1 90101	1 88883
	2	1 95979	1 99249	2 0	1 99605	1 98769	1 97698	1 96611	1 95461	1 94530	1 93547
	3	1 93330	1 97869	1 99605	2 0	1 99701	1 99084	1 98347	1 97497	1 96741	1 95926
	4	1 90641	1 96171	1 98769	1 99701	2 0	1 99811	1 99423	1 98871	1 98314	1 97691
	5	1 88176	1 94450	1 97698	1 99084	1 99811	2 0	1 99884	1 99565	1 99170	1 98702
	6	1 86052	1 92862	1 96611	1 98347	1 99423	1 99884	2 0	1 99876	1 99626	1 99295
	7	1 83982	1 91274	1 95461	1 97497	1 98871	1 99565	1 99876	2 0	1 99871	1 99655
	8	1 82601	1 90101	1 94530	1 96741	1 98314	1 99170	1 99626	1 99871	2 0	1 99873
	9	1 81174	1 88883	1 93547	1 95926	1 97691	1 98702	1 99295	1 99655	1 99873	2 0
8	0	2 0	1 98564	1 95880	1 92914	1 90196	1 87378	1 84979	1 82513	1 80692	1 78422
	1	1 98564	2 0	1 99262	1 97712	1 95970	1 93977	1 92168	1 90182	1 88675	1 86770
	2	1 95880	1 99262	2 0	1 99547	1 98600	1 97296	1 95994	1 94460	1 93244	1 91684
	3	1 92914	1 97712	1 99547	2 0	1 99694	1 98973	1 98112	1 96988	1 96042	1 94787
	4	1 90196	1 95970	1 98600	1 99694	2 0	1 99669	1 99147	1 98352	1 97622	1 96622
	5	1 87378	1 93977	1 97296	1 98973	1 99669	2 0	1 99674	1 99146	1 98585	1 97877
	6	1 84979	1 92168	1 95994	1 98112	1 99147	1 99674	2 0	1 99727	1 99361	1 98768
	7	1 82513	1 90182	1 94460	1 96988	1 98352	1 99146	1 99727	2 0	1 99831	1 99363
	8	1 80692	1 88675	1 93244	1 96042	1 97622	1 98585	1 99361	1 99831	2 0	1 99615
	9	1 78422	1 86770	1 91684	1 94787	1 96622	1 97877	1 98768	1 99363	1 99615	2 0
9	0	2 0	1 98531	1 95628	1 92447	1 89367	1 86533	1 84634	1 82355	1 80309	1 78477
	1	1 98531	2 0	1 99147	1 97515	1 95535	1 93521	1 92066	1 90285	1 88630	1 87107
	2	1 95628	1 99147	2 0	1 99437	1 98372	1 97066	1 96023	1 94698	1 93408	1 92182
	3	1 92447	1 97515	1 99437	2 0	1 99697	1 98996	1 98273	1 97359	1 96405	1 95458
	4	1 89367	1 95535	1 98372	1 99697	2 0	1 99795	1 99359	1 98789	1 98124	1 97418
	5	1 86533	1 93521	1 97066	1 98996	1 99795	2 0	1 99807	1 99533	1 99116	1 98620
	6	1 84634	1 92066	1 96023	1 98273	1 99359	1 99807	2 0	1 99887	1 99612	1 99242
	7	1 82355	1 90285	1 94698	1 97359	1 98789	1 99533	1 99887	2 0	1 99915	1 99710
	8	1 80309	1 88630	1 93408	1 96405	1 98124	1 99116	1 99612	1 99915	2 0	1 99937
	9	1 78477	1 87107	1 92182	1 95458	1 97418	1 98620	1 99242	1 99710	1 99937	2 0

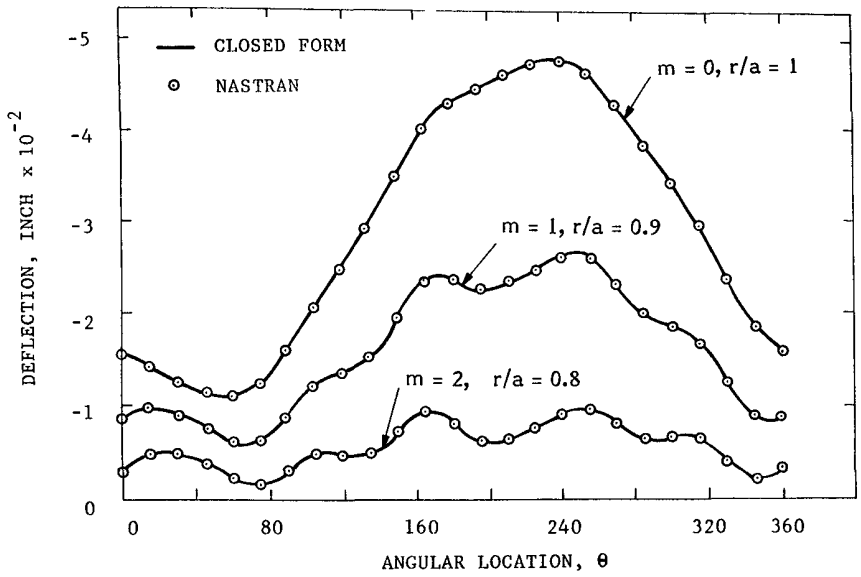

(a) Mirror configuration:

R = radius of curvature

= 250"

a = 50"

b/a = 0.2

E = 10^7 psi

D = 13.4 x 10^6 lb. in.

ν = 0.17

(b) Mirror configuration:

same as in (a),

except that b/a = o

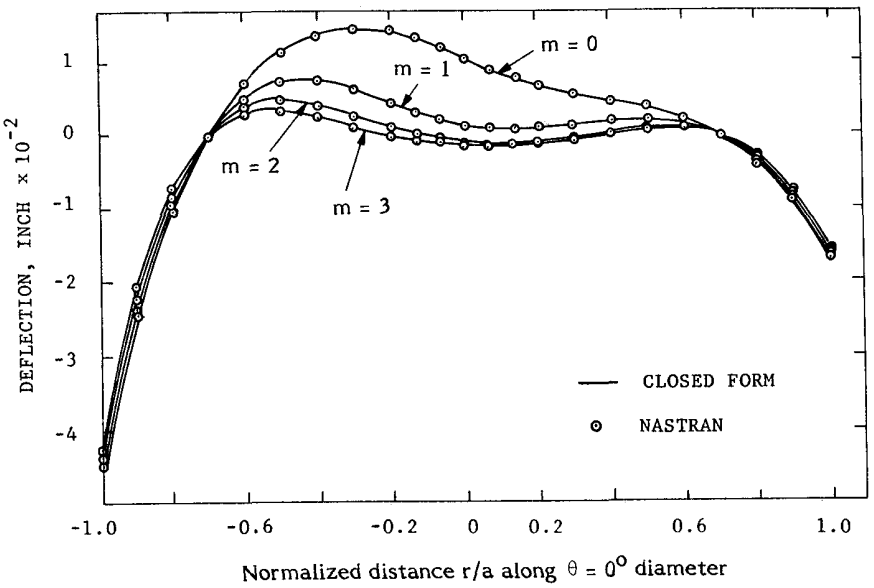

Figure 7. Test run correlation between Nastran and closed form solutions for a curved circular mirror subjected to the thermal moment distribution of Figure 4.

Acknowledgements

The work presented in this paper was performed under an IR&D authorization of the Perkin-Elmer Corporation.

References

1. Boley, Bruno A. and Weiner, Jerome H., Theory of Thermal Stresses, John Wiley & Sons, Inc. (1960).

2. Mehta, Pravin K., "Non-symmetric Thermal Bowing of Kinematically Mounted Flat Circular Optical Elements", Tech. memo. PKM-0104, The Perkin-Elmer Corporation (10/20/1983).

3. Reissner, E., "Stresses and Small Displacements of Shallow Spherical Shells", J. Math. Phy. 25, 80-85, 279-300 (1946); also 27, 240 (1948); and 38, 16-35 (1959).

4. Krauss, H., Thin Elastic Shells, John Wiley & Sons, Inc. (1967).